IEPC-95-240

Two-Dimensional Hybrid Particle-In-Cell (PIC) Modeling of Hall Thrusters *

John Michael Fife† and Manuel Martinez-Sanchez‡
Massachusetts Institute of Technology
Cambridge, Massachusetts

A two dimensional numerical simulation was written for the acceleration channel and near plume of a Hall thruster, and the results were compared with experimental measurements. The model assumes quasineutrality, Maxwellian electrons, and Bohm diffusion across the magnetic field lines. Heavy particles are simulated directly with a Particle-In-Cell (PIC) method, while electrons are modeled as a fluid continuum. A time-accurate electron energy equation is used to determine electron temperature, and a generalized Ohm's Law is used to determine the electric field strengths. Results indicate a strong correlation with experimental performance data. In particular, the simulation is able to predict thrust, torque, power, and efficiency to within 7% of the experimental values. In addition, wall erosion rates in the Russian SPT can be predicted to within 40% using a simple analysis of the simulation results. Two-dimensional plasma distributions are similar to experiment, but do not match in all cases. This is most likely due to the general Bohm diffusion model applied globally to the Hall thruster plasma.

Introduction

In 1992, Lentz [1] used a one-dimensional numerical model to accurately predict the operating characteristics and plasma parameters in the acceleration channel of a Japanese Type II Hall Thruster. The assumptions of the Lentz model included quasineutrality, Bohm diffusion across the magnetic field, constant ratio of ionization energy loss to total electron energy loss, and fixed magnetic field.

Due to the success of the Lentz one-dimensional model, this research extends the model to two dimensions, using similar assumptions. The physical dimensions are considered an input to the numerical model, so any Hall thruster geometry may be used, as well as concept designs. A computational grid is mapped to physical space using nonuniform mapping techniques common in computational fluid mechanics. The magnetic field is pre-computed from the iron pole locations and solenoid strengths. Electrons are modeled as a Maxwellian Fluid, while the heavy species are treated with a modified Particle-In-Cell (modified PIC) methodology. Collisionality is limited to electron-neutral ionization and ion-neutral momentum exchange. The overall scheme may be called "hybrid-PIC" since both fluid and PIC methods are used self-consistently.

This paper describes the governing equations and numerical method used in modeling the Hall Thruster in two dimensions. Results are then explained, and comparisons are made with experimental data for Russian SPT-class thrusters.

*Supported under AFOSR grant no. 91-0256
†Ph.D. Candidate
‡Professor

Governing Equations

0.1 Magnetic Field

The magnetic field is considered equal to the vacuum field, and hence expressible as $\vec{B} = \nabla\sigma$. Since $\nabla \cdot \vec{B} = 0$, it is also possible to define a magnetic stream function whose gradient is everywhere orthogonal to $\vec{B}$. One such stream function is λ, given by

$$\frac{\partial \lambda}{\partial z} = r\frac{\partial \sigma}{\partial r} = rB_r \quad (1)$$

$$\frac{\partial \lambda}{\partial r} = -r\frac{\partial \sigma}{\partial z} = -rB_z \quad (2)$$

If $\hat{n}$ is the distance normal to the magnetic field lines, then,

$$\frac{\partial}{\partial \hat{n}} = \frac{\partial \lambda}{\partial \hat{n}}\frac{\partial}{\partial \lambda} = -rB\frac{\partial}{\partial \lambda} \quad (3)$$

Electron Momentum Balance

Along lines of force, the electrons are assumed to lie in Boltzmann equilibrium with constant electron temperature

$$\phi - \frac{kT_e}{e}\ln(n_e) = \phi^*(\lambda) \quad (4)$$

Across lines of force, a force balance on electrons may be written as

$$\nabla P_e = -en_e\vec{E} + m_e n_e \nu_{ei}(\vec{u}_i - \vec{u}_e) \quad (5)$$

where ν_{ei} is the electron-ion collision frequency. Rewriting in terms of the electron mobility, μ_e, and taking only the component normal to the magnetic field lines,

$$u_{e,\hat{n}} = \mu_e\left(\frac{\partial \phi}{\partial \hat{n}} - \frac{kT_e}{en_e}\frac{\partial n_e}{\partial \hat{n}} - \frac{k}{e}\frac{dT_e}{d\hat{n}}\right) + u_{i,\hat{n}} \quad (6)$$

Bohm Diffusion

Assuming Bohm diffusion,

$$\mu_e = \frac{1}{16B} \quad (7)$$

Applying this Bohm mobility to Equations (4) and (6),

$$\frac{\partial \phi}{\partial \hat{n}} = -rB\frac{d\phi^*}{d\lambda} + \frac{kT_e}{en_e}\frac{\partial n_e}{\partial \hat{n}} - \frac{rBk\ln(n_e)}{e}\frac{dT_e}{d\lambda} \quad (8)$$

$$u_{e,\hat{n}} = -\frac{r}{16}\frac{d\phi^*}{d\lambda} - \frac{kr}{16e}(\ln(n_e) - 1)\frac{dT_e}{d\lambda} + u_{i,\hat{n}} \quad (9)$$

Current Conservation

To conserve current, $I_a = I_e + I_i$, independent of λ. Written in terms of integrals along magnetic field lines,

$$I_a = 2\pi e\int_0^l n_e u_{e,\hat{n}} r\,ds - 2\pi e\int_0^l n_i u_{i,\hat{n}} r\,ds \quad (10)$$

Using Equation (8) and simplifying,

$$\frac{d\phi^*}{d\lambda} = \frac{-I_a - \frac{2\pi k}{16}\frac{dT_e}{d\lambda}\int_0^l n_e(\ln(n_e) - 1)r^2\,ds}{\frac{2\pi e}{16}\int_0^l n_e r^2\,ds} \quad (11)$$

Electron Energy

An electron energy equation may be derived under the assumptions that electrons have a Maxwellian velocity distribution and that the pressure dyad reduces to a scalar pressure term, $n_e kT_e$:

$$\frac{\partial}{\partial t}\left(\frac{3}{2}n_e kT_e\right) + \nabla\cdot\left(\frac{5}{2}n_e\vec{u}_e kT_e + \vec{q}_e\right) = S \quad (12)$$

Here, the directed kinetic energy of electrons is neglected, since, for Hall thrusters, this is found to be smaller than the random kinetic energy.

In Equation (12), S is the electron energy source due to ionization, radiation, and charge-field interactions. The net energy cost for producing a single ion, φ, can be expressed as the sum of the energy required for ionization, plus the energy lost to excitation of neutral atoms. An analytical expression for φ is derived by Dugan et. al. [2]. The result can be fitted closely as,

$$\varphi' = Ae^{-\frac{B}{z}} + C \quad (13)$$

where φ' and z are normalized ion production cost and dimensionless electron kinetic temperature, $\varphi' = \frac{\varphi}{E_i}$ and $z = \frac{kT_e}{E_i}$. The constants A, B, and C are given in Table 1. The volumetric electron energy loss rate can then be given as,

$$S_1 = \dot{n}_e\varphi' E_i \quad (14)$$

The electron energy source due to the electric field is shown [3] to be,

$$S_2 = \frac{16Bj^2}{en_e} \quad (15)$$

	A	B	C
Argon	0.188	0.624	1.75
Xenon	0.254	0.677	2.00

Table 1: Constants to fit the Dugan ion production cost model.

Combining the sources explicitly,

$$S = -\dot{n}_e \varphi' E_i + \frac{16 B j^2}{e n_e} \tag{16}$$

Heavy Species

Heavy species are modeled as discrete particles with negligible temperature. Therefore, only conservation of mass and momentum are applicable. Recombination and charge exchange are found to be small and both are neglected. The ion-neutral collision cross section for argon and xenon are assumed to be 1.40×10^{-18} and 2.15×10^{-18}, respectively. Using these values with experimental Hall thruster plasma densities, the mean free path for both ions and neutrals is found to be large in most regions. Therefore, ion-neutral momentum exchange is neglected.

The magnetic part of the Lorentz force is ignored, since the Larmor radius for ions is large. Therefore, the force on an ion is simply,

$$\vec{F}_i = e\vec{E} \tag{17}$$

Neutrals, being uncharged, only experience velocity changes if they encounter walls. Their mean free path is large compared to the scale of the device.

Ionization Rate

In this model, it is assumed that only electron-neutral collisions can produce ions. Also, it is assumed that only one degree of ionization may exist. Therefore, $\dot{n}_i = \dot{n}_e$.

The nonelastic ionization cross section is approximated according to Drawin [4] as a function of electron energy. Assuming a Maxwellian electron distribution, the resulting expression may be written as,

$$\dot{n}_e = n_e n_n \varsigma(T_e) \tag{18}$$

where ς is plotted for argon and xenon versus electron temperature in Figure 1.

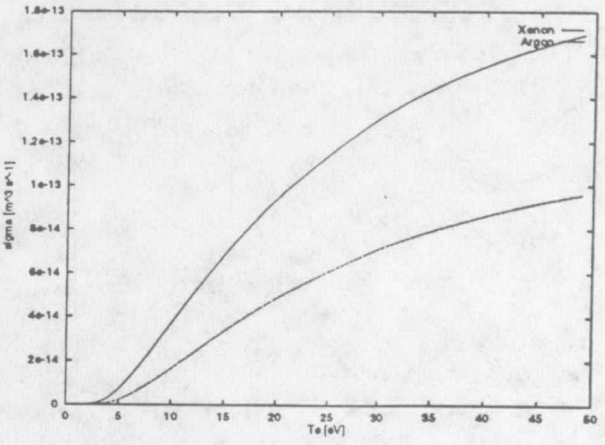

Figure 1: Ionization rate parameter, ς $[m^3 \cdot^- 1]$, for argon and xenon.

Boundary Conditions

To determine the electron energy loss to the walls, it is assumed that the electron flux is equal to the ion flux normal to the wall, and that all ions recombine there with no secondary electron emission. Therefore, the electron energy flux to the wall is simply,

$$E_w = 2kT_e\Gamma_{i,w} \tag{19}$$

All neutrals are assumed to deflect off the walls elastically, at random angles. Likewise, ions recombine at the wall to form neutrals with random direction and velocity magnitudes equal to the impinging ion's.

The cathode and anode are assumed to be at a constant potential difference. Also, the electron temperature at the cathode is fixed, based on experimental data, to $2eV$. The electron temperature at the anode is assumed to have zero slope. The inner and outer walls of the thruster are assumed to be electrically insulating.

Neutrals are assumed to enter the acceleration channel at the injector. The injector is modeled as an annular ring in the center of the back wall (anode) of the channel. The total area of the injector is set roughly to the injector area of the device being modeled. However, precise data is not available for the SPT,

so the injector area is set to approximately 30% of the anode area.

Neutrals are introduced with an axial velocity equal to the speed of sound ($\sqrt{\frac{5kT_e}{3m_n}}$) at the anode temperature (1000 $^\circ K$ for the SPT). The radial velocity component for each neutral is taken to be a random value between $-|v_z|$ and $|v_z|$, where $|v_z| = \sqrt{\frac{2kT_n}{\pi m_n}}$ is the mean directional velocity for a Maxwellian fluid.

The thruster is assumed to have an ideal power supply which maintains constant discharge potential while allowing the discharge current to vary. However, if the power level exceeds a given point (1 kW for the SPT operating at 200 Volts), it goes into a power limiting mode which drops the discharge potential accordingly.

Numerical Method

On the heavy particle time scale, a time-accurate solution to the governing equations can be achieved by iterating successively, as shown in Figure 2.

A 51 × 13-node nonuniform spatial grid is used. Rotational symmetry is assumed. Therefore, only a meridional section of the Hall thruster is modeled. Grid spacing is determined by the timestep of the simulation. It is set to the smallest value which is much larger than the maximum distance traveled by a particle in one timestep. Figure 3 shows the spatial grid used for the computations presented in this paper.

Magnetic Field

The magnetic field is pre-computed by specifying the geometry of the iron poles (which are assumed to have infinite permeability), and solving Laplace's equation on the regions exterior to them. The method of red-black ordering was found to be the most flexible. Solutions take 8 hours on a DEC Alpha workstation, but programming is minimal and it works for a variety of axisymmetric geometries.

Integration of Electron Equations

It is possible to combine the electron energy equation with Ohm's Law and the electron

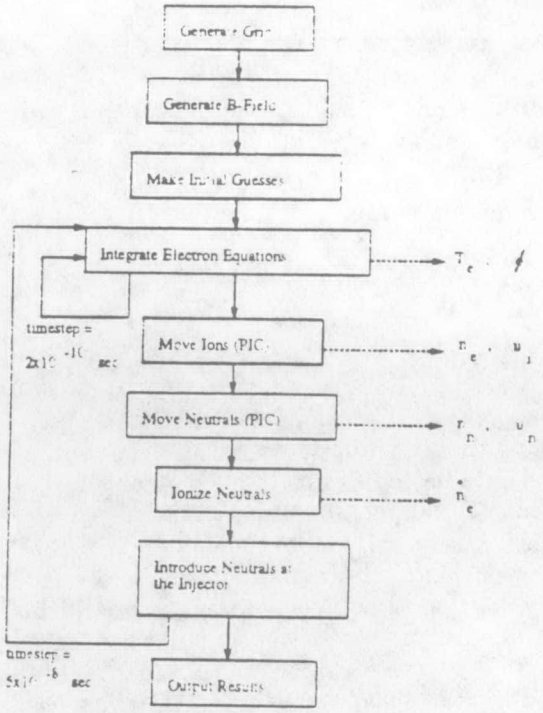

Figure 2: Overview of the numerical method.

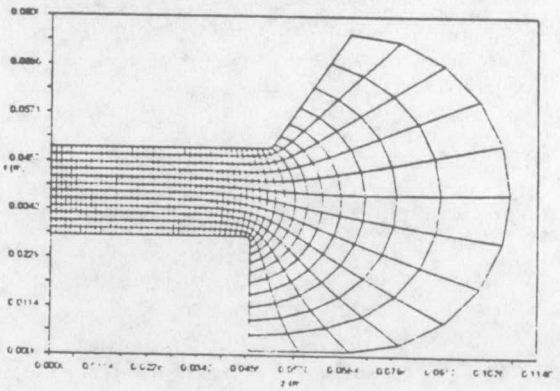

Figure 3: Spatial grid for the SPT-100 geometry.

current equation. The result is of the form:

$$\frac{\partial T_e}{\partial t} - \bar{I}\frac{\partial T_e}{\partial \lambda} + \bar{J}\left(\frac{\partial T_e}{\partial \lambda}\right)^2 + \bar{K}\frac{\partial T_e}{\partial \lambda}T_e - \bar{L}T_e + \bar{M}T_e^2 + \bar{N} + \bar{O}T_e\frac{\partial^2 T_e}{\partial \lambda^2} = 0 \quad (20)$$

where $\bar{I}, \bar{J}, \ldots \bar{N}$ represent factors obtained by itegrating along magnetic field lines from the inner to the outer wall. This equation is a function of slow time parameters and of the electron temperature. The slow time parameters are taken to be those related to heavy particle motion (n_e, n_n and v_i), and those fixed geometrically (B, r). Holding the slow parameters constant, this equation is solved time-accurately for electron temperature, which evolves faster, using MacCormack's method. The space potential can then be found on the whole domain by using Boltzmann equilibrium and Ohm's Law.

PIC Method for Heavy Species

In this simulation, heavy species are modeled time-accurately using a modified Particle-In-Cell (PIC) method. The standard PIC method [5] is a direct simulation technique which models a gas as discrete particles. Figure 4 shows the operation of one standard PIC cycle.

The method used here has several unique features which enhance performance for the specific problem of simulating a Hall thruster plasma with a nonuniform grid:

- Fluid equations and quasineutrality determine fields, not Poisson's equation. This allows spatial scales much greater than the Debye length.
- PIC superparticles may have variable mass.
- Computational coordinates for each particle are maintained with a unique particle following algorithm based upon Newton's method

Complete cases take 20 hours to execute on a DEC Alpha workstation.

Convergence

Since the method is time-accurate, there is no guarantee that the system will converge to a steady state solution. Two types of instabilities may prevent convergence:

- Plasma instabilities due to convection and diffusion of electrons and ions, combined with ionization kinetics
- Numerical "noise" due to the limitations of the PIC method in simulating a continuum of heavy particles

The parameters are averaged over a long time scale, and iteration is stopped when the averages reach a constant value. The time it takes for convergence is assumed to be, at the very minimum, the time for convection of slow neutrals along the length of the grid.

Results and Discussion

Bishaev and Kim used diagnostic probes to measure plasma parameters in the acceleration channel of a Hall thruster. The results in this paper have been obtained with a simulated geometry which closely matches what they reported [6]. The operating conditions are given in Table 2.

Operating Parameters for the SPT	
Propellant	Xenon
ϕ_d	200 Volts
$\dot{m}$	3 mg/s
Vacuum	2×10^{-4} Torr
$B_{r,max}$	.018 Tesla

Table 2: Operating conditions for the Bishaev/Kim SPT experiments.

The magnetic field parameters are shown on the computational domain in Figures 5 and 6. Although the radial magnetic field strength is close to the experimental value, the contours of magnetic flux are not matched exactly. This is due to differences in iron pole geometry, as well as to the infinite permeability and ideal solenoid assumptions used in the numerical model.

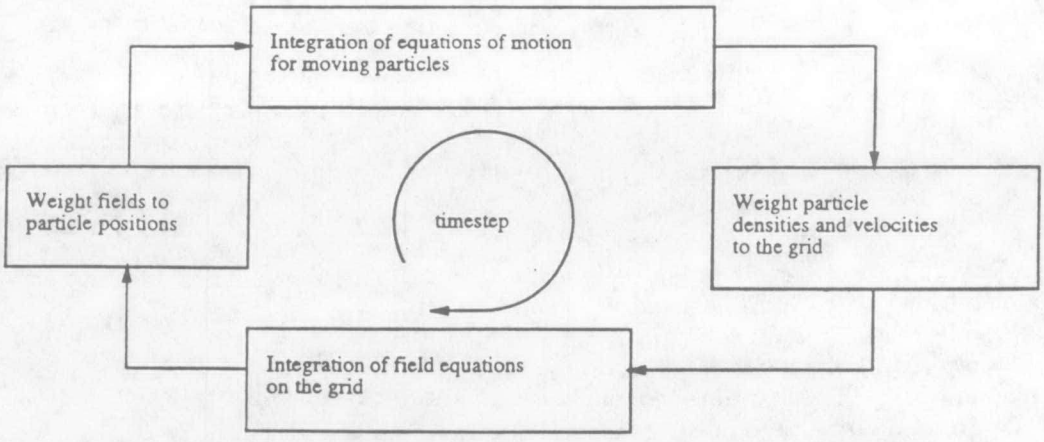

Figure 4: PIC computational cycle [5].

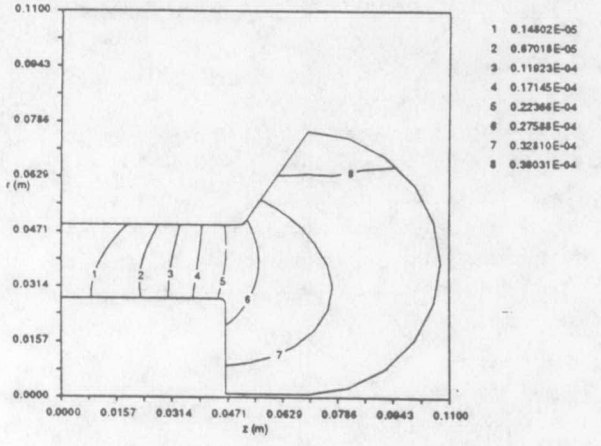

Figure 5: Magnetic stream contours, λ $[T \cdot m^2]$, computed for the Bishaev/Kim SPT geometry. The contour numbers correspond to the values of λ listed in the key.

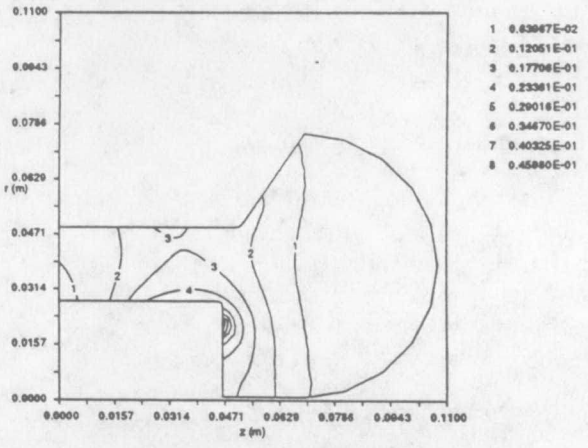

Figure 6: Magnitude of the magnetic field, B $[T]$, computed for the Bishaev/Kim SPT geometry. The contour numbers correspond to the values of B listed in the key.

Performance

Although the Bohm diffusion coefficient is generally written as,

$$D_{Bohm} \approx \frac{kT_e}{16eB} \qquad (21)$$

it is known to vary by an order of magnitude depending upon the plasma parameters. Therefore, the simulation was run for three cases to isolate the best fit for the Hall thruster. A constant K_{Bohm} was introduced as a multiplier,

$$D_{Bohm} \approx K_{Bohm} \frac{kT_e}{16eB} \qquad (22)$$

and the simulation was run for $K_{Bohm} = 0.75$, 1.0, and 1.25. After convergence, the results were averaged in time. Results are shown in Table 3.

It is interesting to note that, for the model used, varying K_{Bohm} is equivalent to inversely

varying B. This is due to the form of the Bohm conductivity. K_{Bohm} and B always appear in the model together as $\frac{K_{Bohm}}{B}$.

The first case ($K_{Bohm} = 0.75$) shows the effect of "quenching" the device with more propellant than is possible to ionize. At low K_{Bohm}, the power input to the electrons is lower, and ionization rate is reduced. The higher neutral density acts as an energy sink, keeping the electron temperature low and reducing the ionization rate further. This is self-perpetuating, since the ion production cost increases at lower energies, as seen in Equation (13).

In the second case, the anode current matches the experimental value almost exactly. The efficiency of this model reproduces the advertised efficiency of the SPT-100, which is 50%. The specific impulse is also a close match with experimental data. This is not surprising, since the discharge potential was fixed to the same value measured, and the simulation reached full propellant utilization.

The third case, $K_{Bohm} = 1.25$, represents the effect of reduced electron impedance. The higher electron mobility increases their heating rate. This moves the ionization region toward the anode, increasing the ion wall losses.

The Bohm diffusion mechanism is not well understood. It is an empirical fit with some uncertainty. Therefore, it is surprising that the standard case fits the experimental performance data so well. Furthermore, it is curious that the correlation degrades so rapidly as K_{Bohm} deviates from unity, particularly on the low side.

Two-Dimensional Results

Figures 7 through 13 show the time-averaged two-dimensional results for the case $K_{Bohm} = 1.0$. Some discrepancies exist between the experimental data of Bishaev and Kim, and the results of the two-dimensional simulation. The potential at the exit of the channel is found experimentally to be 10 Volts, whereas the numerical model predicts it to be 118 Volts. This discrepancy may be due to the location of the cathode. The simulation cathode is assumed to be located about 2.3 cm downstream of the channel. For the experiments of Bishaev and Kim, it may have been located closer. Vacuum chamber back-pressure was thought to cause this, but it was ruled out by numerically modeling the neutral particle flux from the chamber. The effect was negligible, so chamber back-pressure was ignored. Another explanation may be some type of enhanced electron conductivity in or near the plume which is not being modeled.

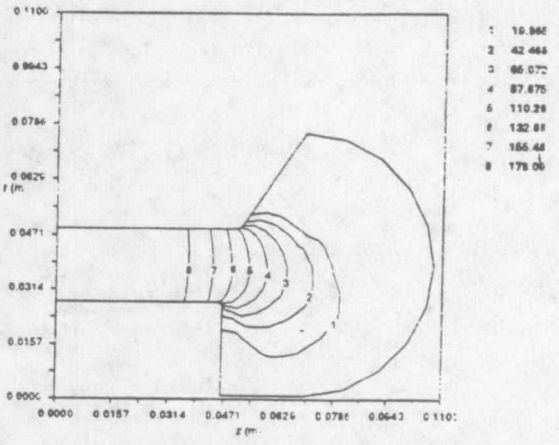

Figure 7: Contours of space potential (ϕ [V/m]) . The contour numbers correspond to the values of ϕ listed in the key. $K_{Bohm} = 1.0$; $\dot{m} = 3$ mg/s; $\phi = 200$ Volts; $I_a = 3.1$ A.

The ion density in Figure 8 also matches poorly with the experimental results. The peak experimental value is about $7 \times 10^{17}\ m^{-3}$ near the exit of the channel. The simulation predicts it to be twice that and to occur closer to the anode.

The assumption of constant electron temperature along lines of force seems to hold only partially. This may imply that the plasma is not entirely in equilibrium along the magnetic lines, and perhaps the Boltzmann relation is not completely applicable. Alternatively, perhaps they are in equilibrium, but an electron energy balance holds instead of Boltzmann's relation. This is a matter under investigation. Nevertheless, the peak electron temperature is predicted correctly.

Also, the temperature gradients are strong in the experimental measurements. This is not the case with the simulation. One reason for this discrepancy may be overprediction

	Experimental	Numerical		
		$K_{Bohm} = 0.75$	$K_{Bohm} = 1.00$	$K_{Bohm} = 1.25$
I_a $[A]$	3.15	0.39	3.10	2.75
I_b $[A]$	2.10	0.52	2.20	1.90
I_{SP} $[s]$	1530	200	1475	1400
F $[N]$	.045	.006	.043	.041
$\eta_u = \dot{m}_i/\dot{m}$	0.95	0.24	1.00	0.86
$\eta_a = I_b/I_a$	0.67	1.33	0.71	0.69
$\eta_e = (e/2m_i\phi_a)(F/I_b)^2$	0.84	0.24	0.71	0.86
$\eta = \eta_u\eta_a\eta_e$	0.54	0.08	0.50	0.51
I_{wall} $[A]$	1.0	0.03	1.1	2.3
ξ_s $[\times 10^{-9}\ m/s]$	7.0	1.2	4.0	3.1
$Torque/(F \cdot r_{mean})$	.02-.08	.037	.031	.035

Table 3: Performance results from the numerical simulation. $\dot{m} = 3$ mg/s; $\phi = 200$ Volts.

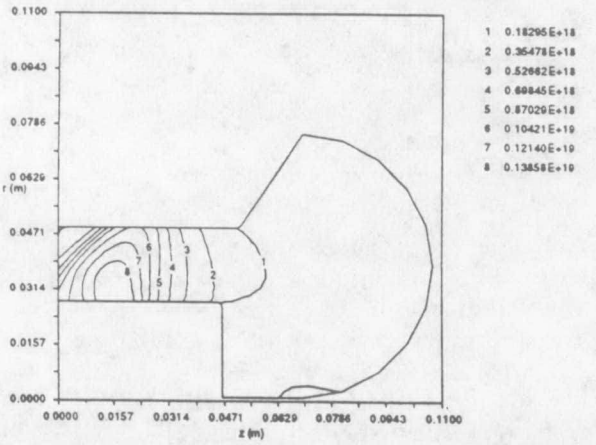

Figure 8: Contours of plasma density (n_i $[m^{-3}]$). The contour numbers correspond to the values of n_i listed in the key. $K_{Bohm} = 1.0$; $\dot{m} = 3$ mg/s; $\phi = 200$ Volts; $I_a = 3.1$ A.

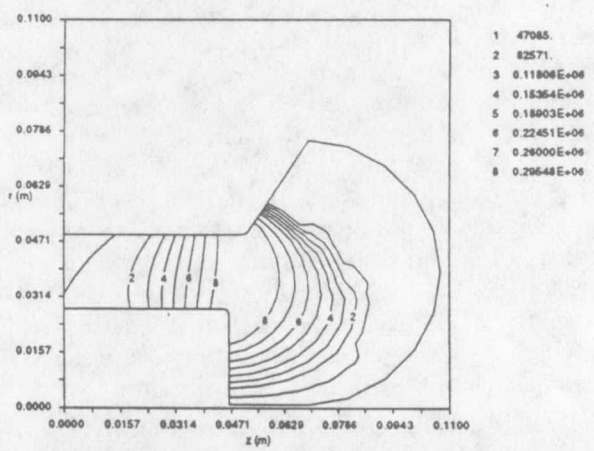

Figure 9: Contours of electron temperature (T_e $[^\circ K]$). The contour numbers correspond to the values of T_e listed in the key. $K_{Bohm} = 1.0$; $\dot{m} = 3$ mg/s; $\phi = 200$ Volts; $I_a = 3.1$ A.

of the thermal diffusion coefficient, which was derived from the Bohm diffusivity.

Experimental measurements of ion flux show most of the flux vectors leaving the region of high plasma density, as expected, and traveling along potential lines or to the walls. The simulation results (Figure 11) show a similar pattern of ion flux, with the vectors emanating from a high density region closer to the anode and closer to the inner wall.

The two-dimensional numerical results are consistent when taken as a set. Electron temperature increases from the cathode to the acceleration zone, since there is little inelastic collision loss in that region due to the low neutral density. Once inside the channel, the electrons enter a region of higher neutral density. Ionization peaks when the neutral density is increasing. Electron temperature then decreases from inelastic losses.

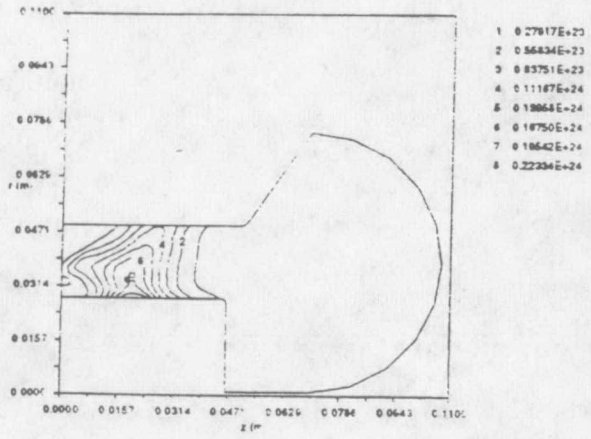

Figure 10: Contours of ionization rate ($\dot{n}_i$ $[m^{-3}s^{-1}]$). The contour numbers correspond to the values of $\dot{n}_i$ listed in the key. $K_{Bohm} = 1.0$; $\dot{m} = 3$ mg/s; $\phi = 200$ Volts; $I_a = 3.1$ A.

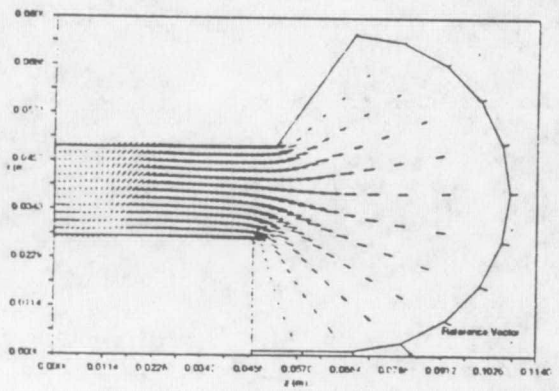

Figure 11: Vectors of ion number flux ($\vec{\Gamma}_i$ $[m^{-2}s^{-1}]$). The reference vector represents a flux of $14.8 \times 10^{20} m^2/s$. The contour numbers correspond to the values of $\vec{\Gamma}_i$ listed in the key. $K_{Bohm} = 1.0$; $\dot{m} = 3$ mg/s; $\phi = 200$ Volts; $I_a = 3.1$ A.

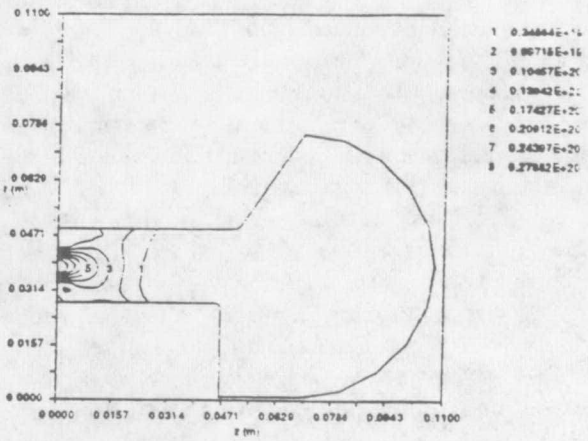

Figure 12: Contours of neutral number density (n_n $[m^{-3}]$). $K_{Bohm} = 1.0$; $\dot{m} = 3$ mg/s; $\phi = 200$ Volts; $I_a = 3.1$ A.

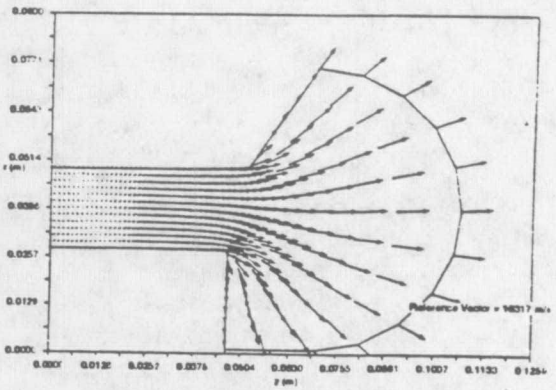

Figure 13: Vectors of ion velocity ($\vec{u}_i$ $[m/s]$). The reference vector represents a velocity magnitude of 16317 m/s. $K_{Bohm} = 1.0$; $\dot{m} = 3$ mg/s; $\phi = 200$ Volts; $I_a = 3.1$ A.

Torque

The torque on the device may be written as the sum of the azimuthal moments on the ions in each grid cell as,

$$T = \sum 2\pi r^2 A_{cell} e n_i \vec{u}_i \times \vec{B} \qquad (23)$$

The torque is generally nonimensionalized by dividing by the thrust and the mean radius. The torque parameters are given in Table 3, and are consistent with experimental estimates [7, 8].

Ion Wall Impingement

From the numerical simulation, average wall impingement current is calculated to be 1.1 Amperes. According to Bishaev and Kim [6], ion loss to the walls is approximately 1.0 Ampere. Ion wall currents for the other cases are also listed in Table 3.

The SPT-100 insulator wall is known to sputter most near the channel exit [9]. Indeed, Figure 13 shows the mean ion velocities at the wall to be a maximum near the exit of the channel. At the inner wall, ion current density is $48A/m^2$ normal to the wall. A comparison of wall sputtering rate can be made by using the relation,

$$\xi_s = j_{i,w} S_v \tag{24}$$

where ξ_s is the wall reduction rate in m/s, $j_{i,w}$ is the normal component of the ion current density, and S_v is the volumetric sputtering coefficient. Abgaryan et. al. [10] measured the sputtering properties of borosil, a dielectric wall material used in SPTs. They found that $S_v \approx .08\ (mm)^3/C$ for ion energies of 33 eV at an 80 degree angle of incidence. Therefore,

$$\xi_s \approx 4 \times 10^{-9} m/s \tag{25}$$

which is very close to the experimental value of wall sputtering for SPTs. At the inner insulator wall, the initial sputtering rate is 7×10^{-9} m/s from experiments by Garner et. al. [9]. The SPT may easily have twice the ion flux at that point, however, in which case the calculated value would be very close. Nevertheless, the order of magnitude analysis agrees with experimental results.

Plasma Oscillations

The Hall thruster simulation does not reach a steady state solution. Plasma parameters fluctuate continually, even after long convergence times. The two-dimensional results presented above have been averaged over .5 ms. The anode current for this period is given in Figure 14. It can be seen that I_a fluctuates $\pm 15\%$. The electron temperature is plotted in Figure 15 for the same time period.

Two of the slow characteristic frequencies in Table 4 can be seen in the data. The lowest frequency, related to the travel of neutrals from the injector to the exit of the channel, appears in Figure 14 as roughly 6 kHz. Also, by examining Figure 15, a clear 28 kHz behavior is seen, possibly due to neutrals traversing the length of the ionization region.

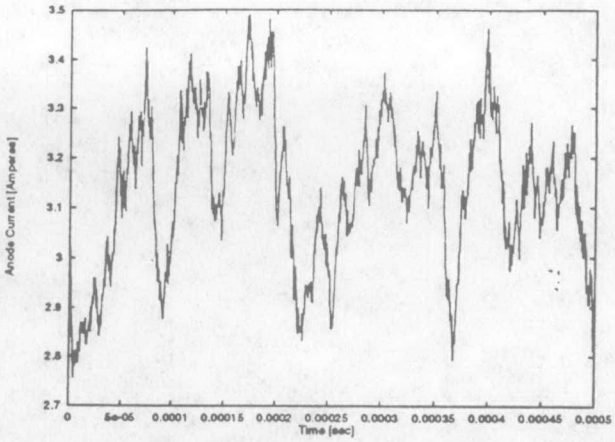

Figure 14: Long time history of anode current, I_a [Amperes].

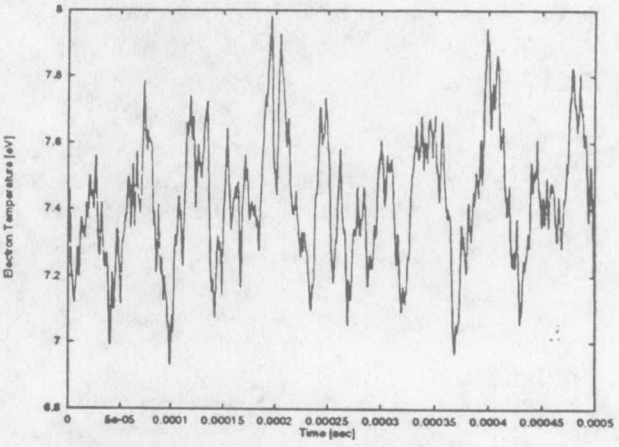

Figure 15: Long time history of electron temperature, T_e $[eV]$, at z = 1.9 cm and r = 3.6 cm.

To closely examine the high frequency oscillations, n_e and n_n have been plotted on a short time scale (.05 ms) in Figures 16 and 17 for a particular node near the peak of ionization rate.

The dominant high frequency information in Figure 16, may be seen to be superimposed

	Velocity, m/s	Distance, cm	Frequency, kHz
Neutrals traverse the channel	300	4	8
Neutrals traverse the ionization region	300	1	30
Ions traverse the channel	3000	4	75
Ions traverse the ionization region	500	1	50
Neutrals traverse two grid cells	300	.24	125
Ions traverse two grid cells	600	.24	250

Table 4: Characteristic frequencies expected.

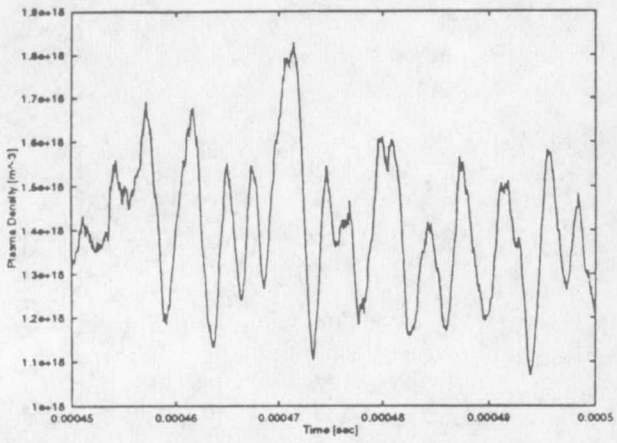

Figure 16: Short time history of plasma density, n_i $[m^{-3}]$, at z = 1.9 cm and r = 3.6 cm.

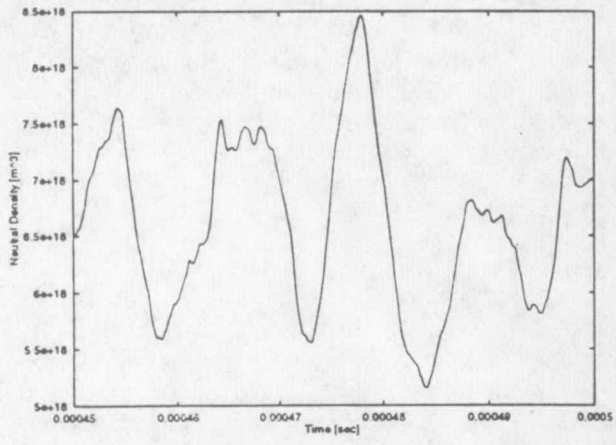

Figure 17: Short time history of neutral number density, n_n $[m^{-3}]$, at z = 1.9 cm and r = 3.6 cm.

on a slower signal which appears to be in the 80 kHz range. This corresponds roughly to the frequency of ions traversing the ionization region.

The high frequency oscillations visible in Figure 16 occur at a frequency of aproximately 300 kHz. The neutral density fluctuations in Figure 17 are at approximately 100 kHz. Both of these high frequency oscillations may be related to the time scale of ion and neutral passage across grid cells, as can be seen in Table 4.

Conclusions

The Hall thruster simulation accurately predicted the performance parameters for the Bishaev/Kim SPT. Efficiency and specific impulse were accurate to within 8%. Anode current and beam current were accurate to within 5%. The net torque on the device was also calculated, and was found to lie within the bounds of experimental measurement. This implies that the numerical model may be very useful in predicting the performance of alternative Hall thruster geometries.

To test the Bohm diffusion assumption, three cases with different Bohm diffusion constants were tried. Surprisingly, the most accurate fit was achieved with a Bohm diffusivity equal to its traditionally quoted value of $\frac{kT_e}{16B}$, even though this is regarded as a rough approximation only.

The two-dimensional numerical results followed similar trends as the experimental values. However, the simulation predicted higher ionization rate near the anode. Also, the electron temperature rise outside the channel was not seen in experimental results.

Total wall impingement current was close to the experimental value. Using the wall current density and an experimental sputtering yield, the wall erosion rate was calculated. Comparing this to experiments with the SPT-100, a close agreement was found.

Therefore, the numerical model was useful for predicting the performance parameters of the Bishaev/Kim SPT geometry. The two-dimensional results lacked close agreement with experiment, but were consistent with the numerical model. The usefulness of the simulation is in predicting the performance, wall erosion rate, and torque of prototype Hall thrusters, and as a tool for understanding the physics of the plasma acceleration process.

Further Work

Work in refining the diffusion model is underway. Experimental investigations of the Hall thruster plasma are needed, in order to generate detailed information about electron currents across and along magnetic field lines. This would allow tabulation of diffusion coefficients as a function of plasma parameters, and more accurate simulation of two-dimensional phenomena.

References

[1] Lentz, C. A., "Transient One Dimensional Numerical Simulation of Hall Thrusters", Massachusetts Institute of Technology, S.M. Thesis, 1993.

[2] Dugan, John V. and Sovie, Ronald J., "Volume Ion Production Costs in Tenuous Plasmas: A General Atom Theory and Detailed Results for Helium, Argon and Cesium." NASA TN D-4150.

[3] Fife, John M., Two-Dimensonal Hybrid Particle-In-Cell Modeling of Hall Thrusters, Master's Thesis, Massachusetts Institute of Technology, May 1995.

[4] Mitchner and Kruger, Partially Ionized Gasses, John Wiley & Sons, New York, 1973.

[5] Birdsal, C. K., and Langdon, A. B., Plasma Physics via Computer Simulation, IOP Publishing Ltd., Bristol, England, 1991.

[6] Bishaev, A. M., and Kim, V., "Local Plasma Properties in a Hall-Current Accelerator with an Extended Acceleration Zone." Soviet Physics, Technical Physics, 23(9):1055-1057, 1978.

[7] Kozubsky, K., "Disturbance Torques Generated by the Stationary Plasma Thruster", AIAA-93-2349, AIAA/SAE/ASME/ASEE 29th Joint Propulsion Conference and Exhibit, Monterrey, California, June 28-30, 1993.

[8] Manzella, David H., "Stationery Plasma Thruster Ion Velocity Distribution", AIAA-94-3141, 30th AIAA/ASME/SAE/ASEE Joint Propulsion Conference, Indianapolis, Indiana, June 27-29, 1994.

[9] Garner, C. E., et. al., "Cyclic Endurance Test of a SPT-100 Stationery Plasma Thruster," 3rd Russian-German Conference on Electric Propulsion Engines and Their Technical Applications, Stuttgart, Germany, July 1994.

[10] Abgaryan, V., et. al., "Calculation Analysis of the Erosion of the Discharge Chamber Walls and Their Contamination During Prolonged SPT Operation," AIAA/ASMA/SAE/ASEE 30th Jpoint Propulsion Conference and Exhibit, Indianapolis, Indiana, June 1994.